Bioreactor and scaffold design for the mechanical stimulation of anterior cruciate ligament grafts

Bio-Medical Materials and Engineering 23 (2013) 225–237
DOI 10.3233/BME-130746
IOS Press

Bioreactor and scaffold design for the mechanical stimulation of anterior cruciate ligament grafts

M. Hohlrieder [a,*], A.H. Teuschl [b,c], K. Cicha [d], M. van Griensven [b], H. Redl [b] and J. Stampfl [d]
[a] *A.M.I. Agency for Medical Innovations, Feldkirch, Austria*
[b] *Ludwig Boltzmann Institute for Experimental and Clinical Traumatology, AUVA Research Center, Vienna, Austria*
[c] *University of Applied Sciences Technikum Wien, Vienna, Austria*
[d] *Institute of Materials Science and Technology, TU Wien, Vienna, Austria*

Received 23 July 2010
Accepted 31 October 2012

Abstract. Various studies have shown that physical stimuli modulate cell function and this has motivated the development of a bioreactor to engineer tissues *in vitro* by exposing them to mechanical loads. Here, we present a bioreactor for the physical stimulation of anterior cruciate ligament (ACL) grafts, whereby complex multi-dimensional strain can be applied to the matrices. Influences from environmental conditions to the behavior of different cells on our custom-made silk scaffold can be investigated since the design of the bioreactor allows controlling these parameters precisely. With the braided design of the presented silk scaffold we achieve maximum loads and stiffness values matching those of the human ACL. Thus, the existent degummed and wet silk scaffolds absorb maximum loads of 2030 $\pm$ 109 N with stiffness values of 336 $\pm$ 40 N/mm.

Keywords: Anterior cruciate ligament, bioreactor, silk, scaffold, mechanical properties

1. Introduction

Anterior cruciate ligament (ACL) reconstruction has become a routine surgical procedure that allows the patient to return to a level of activity in daily routine that would otherwise not be possible. Unfortunately, there is currently no graft or material ideally suited to replace the ACL. The most common procedure today is a reconstruction using tendon autografts (e.g. patellar, hamstring or semitendinosus tendon) [1–4]. However, this involves several difficulties and disadvantages related to explant morbidity, an increased risk of tendonitis and lengthy rehabilitation periods [5,6]. In recent years good results were reported with using allografts [7,8] whereas due to difficulties in the past the replacement of injured ACL with allografts is currently not well established [9,10]. Due to the lack of remodeling processes that normally tendon autografts run through after ACL reconstructions artificial ligaments could provide its maximum strength immediately, whereby a rapid return to a high level of activity could be in all

*Address for correspondence: Martin Hohlrieder, A.M.I. Agency for Medical Innovations, Im Letten 1, 6800 Feldkirch, Austria. Tel.: +43 5522 90505 0; Fax: +43 5522 90505 4026; E-mail: martin.hohlrieder@ami.at.

probability. Furthermore artificial grafts would ensure unlimited availability of the necessary material without weakening particular parts of the body. These facts are good reasons to use an artificial graft. But for reasons such as mechanical failure due to fatigue and abrasive wear, permanent prosthesis has not gained wide acceptance [11–14].

Due to the lack of satisfying clinical options to reconstruct the ACL, we believe that future replacement strategies will rely on tissue engineering approaches. In the approach presented here, a tissue engineered silk scaffold is produced that will be reabsorbed after implantation progressively while newly formed tissue will then perform the task of the native ACL. Initially the cell-seeded silk scaffold should match the mechanical properties of the human ACL. Since silk provides good mechanical properties as well as beneficial degradation behaviour *in vivo*, silk has gained interest as a scaffold material for tissue engineering applications in recent years [15–17]. Natural silk is composed of a filament core protein, silk fibroin, and a glue-like coating consisting of sericin proteins. Sericin has been found to elicit adverse immune responses associated with silk scaffolds [18]. However, after sericin removal (degumming) regenerated silk shows good biocompatibility, hemocompatibility, oxygen and water permeability [19]. As an FDA-approved biomaterial, silk is degraded and absorbed *in vivo* over a period of one year [18]. Various studies describe the potential of native silk fibroin fibres as three-dimensional scaffolds for tissue engineering of the ACL [15,16,19].

Modern bioreactors are an essential requirement for tissue engineering approaches to better simulate some of the complex *in vivo* conditions [20,21]. A systematic study of cell growth and differentiation into functional tissue becomes feasible. To facilitate reproducible tissue growth, the environmental conditions (e.g. temperature, humidity) and influences from culture medium (pH, pO_2, growth factors and nutrients) need to be controlled precisely. Significant focus has to be given on the mechanical loads which act on the scaffold. Various studies [22–26] have shown that mechanical stimulation significantly influences the proliferation and differentiation of cells. The majority of bioreactors in the tendon and ligament tissue engineering field are designed to allow cell-seeded collagen gels to be cyclically stretched [27–31]. Only a few bioreactors described in literature can be used to study the effects of cells on a pre-structured three-dimensional structured ligament or tendon graft [20,21,27,28,30]. Even fewer studies describe bioreactors capable of mechanically loading silk scaffolds of braided design [32]. Here we describe the development of a high capacity bioreactor with which we can investigate cell-seeded three dimensional scaffolds for tissue engineered ACL grafts [33]. Well-controlled and combined cyclical axial strain and cyclical rotational strain can be applied to three dimensional matrices.

2. Materials and methods

2.1. Bioreactor construction and reactor vessels

The design and construction of the bioreactor (Figs 1 and 2) can be subdivided into five subsystems: (1) the basic structure of the bioreactor, (2) the reactor vessels, (3) the electrical drives with motion control software, (4) the pump system for fluidic control and (5) the incubator to control gas mixture in the cell culture medium.

This bioreactor is capable to cyclically stretch and rotate the scaffolds housed in ten independently working reactor vessels. The framework construction comprises a vertically movable plate. Metal sheets are mounted on their long sides to prevent excessive deflection under load. At the same time the gear wheels are protected from undesirable contact. The reactor vessels are located between this floating plate

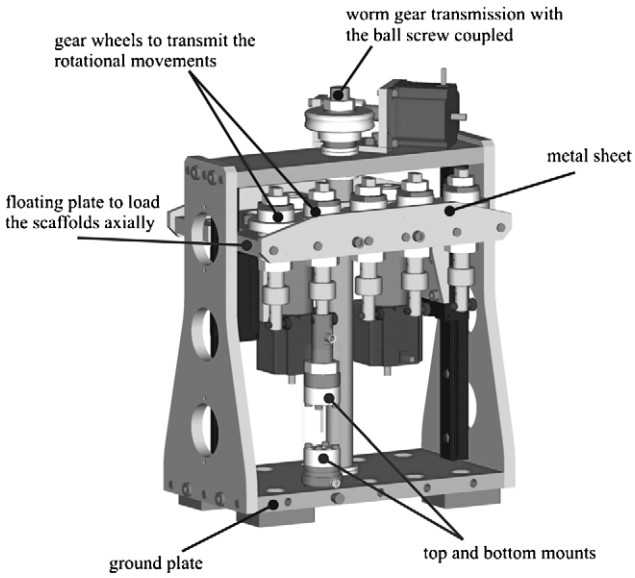

Fig. 1. CAD model of the bioreactor.

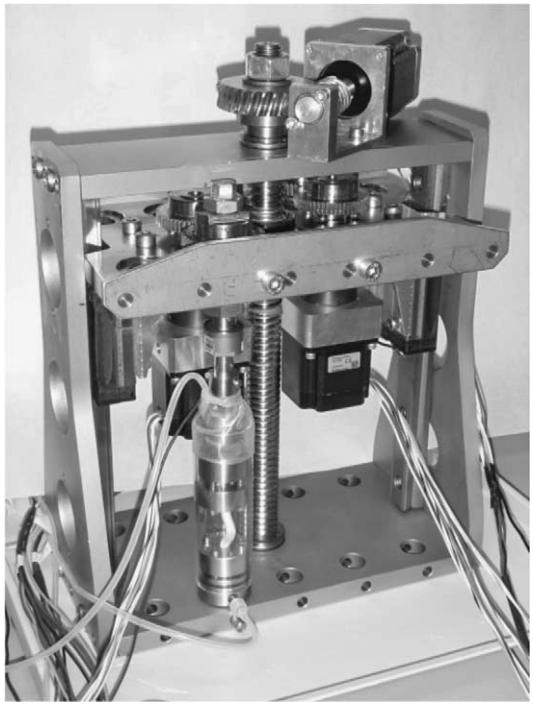

Fig. 2. Image of the bioreactor with one vessel installed.

and the ground plate. Due to the linear motion of the floating plate, the matrices can be loaded axially. Linear bearings are incorporated to minimise friction and guarantee longevity. Rotational displacements of the scaffolds are achieved by an elaborate drive system, which is mounted on top of the floating plate. Each scaffold can be pre-tensioned independently by an intelligent tensioning system (Fig. 3). Over each vessel position a hex nut can be tightened to a desired extent, whereas an anti-twist protection inhibits a rotation of the matrix. Very small pitches of the threads facilitate infinitesimal adjustments of the clamping length, allowing exact tension of the scaffolds. At each vessel position a load cell is mounted coaxially with the matrix. The applied axial load during pre-tensioning or testing can thereby be recorded.

The reactor vessels allow multi-dimensional strain on the matrix while the vessel is sealed completely to avoid contamination. Each vessel is comprised of top and bottom mounts, which allow stable anchoring of a wide range of different scaffold designs. Thereby the ends of the scaffold are compressed between two locking rings, which are axially screwed together with four screws. This ensures a safe and rigid fixation of the scaffold without damaging its structure. Inside the top mount a needle is fixed which penetrates the scaffold in its axis. Thus, culture medium is guided into the inner structures of the matrix as well. Luer-lock adapters are installed at the perfusion in- and outlets, located at the top and bottom mounts, guaranteeing an easy handling. The vessel is encased with a glass tube completely filled with culture medium and is sealed with an O-Ring at the bottom mount. Sealing at the top mount is more challenging because the mechanical manipulations have to be transmitted from the exterior of the vessel to the interior without any frictional loss. Therefore we used a flexible and custom-made silicone tube which allows movement and avoids contamination from outside during testing. This MED4860 silicone (NuSil Technology Europe, Mougins, France) was of medical grade and was tested for cytotoxicity using

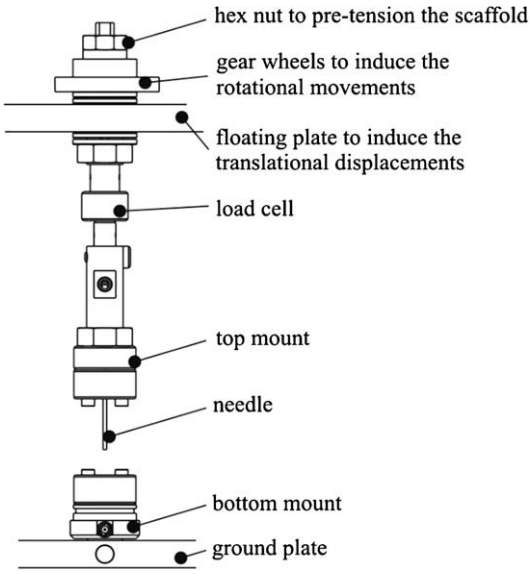

Fig. 3. Schematic illustration of a vessel (without glass tube) and its tensioning system.

a common MTT ([3-(4.5-dimethylthiazol-2-yl)-2.5-diphenyl-tetrazolium bromide]) assay. No cytotoxic effects of this silicone were found (data not shown).

Vessels can be attached and detached independently, which facilitates easy and flexible handling of the samples during sterilization and testing without the need of entire system shutdown. Furthermore the single parts of the vessels can be assembled under sterile conditions using a laminar air-flow bench. Samples can be independently prepared while others are already in the bioreactor for testing. All parts used within the vessel are autoclavable.

2.2. Electrical drives and motion control

Independently working stepper motors enable uncoupled axial and rotational displacements of the scaffolds. Stepper motors, power amplifiers and the power supply unit were purchased from Nanotec GmbH & Co. KG, Landsham, Germany. One stepper motor is placed on top of the framework of the bioreactor and activates a worm gear transmission with a reduction of 1 : 10. The driven shaft of the worm gear transmission is coupled to a ball screw (with a pitch of 5 mm/turn), transforming the rotational movement into a linear motion. Hence, a floating plate moves vertically and enables cyclic axial loading to the matrix. The combination of the worm gear transmission and the ball screw results in infinitesimal axial translation. Based on the characteristics of the ball screw and the worm gear transmission, a maximum axial load of 1000 N can be reached in each vessel. For that purpose the stepper motor has to provide a torque of 0.8 Nm.

All of the components, which are required to induce the rotational displacements, are located on the floating plate. To increase the number of possible testing parameters, rotational movements of the vessels can be applied by two further stepper motors. Each stepper motor controls for every five sections on each bioreactor side. To reduce the total height of the bioreactor, these actuators are mounted on the lower surface of the floating plate. A planetary gear with a ratio of 1 : 12 is flanged directly onto each motor. Gear wheels translate the torque from the driven shaft of the planetary gear to all vessel positions. Therefore, each gear is aligned coaxially with the reactor vessels. A minimum torque of 2 Nm

can hence be provided at each vessel position. To minimize friction, all shafts, including the ball screw, are mounted with thrust ball bearings.

Resolutions of 3 μm for translational and 0.0075° for rotational movements can be achieved. In our investigations, the scaffolds were loaded under 45° rotational and 3.5 mm translational deformations at 66.7 mHz.

To precisely control the movements of the three stepper motors, a user-friendly operator interface is programmed using LabVIEW™ (National Instruments Virtual Instrumentation, Austin, TX). This software provides independent control for rotational and translational movements. Parameters for motion control of the three stepper motors can be set easily; translational movements can be entered in mm and rotational displacements in degrees. Furthermore the software allows the user to set and monitor run cyclic motions on the operator interface in number of cycles/min for the duration of an experiment. In the same way, the force path over time can be monitored online and recorded via load cells (Nanotec GmbH & Co. KG, Landsham, Germany).

Hardware components for power supply and necessary modules for the motion control of the stepper motors are combined in a cubicle of electronic equipment. The front panel comprises a number of sockets for an easier handling.

2.3. Environmental and fluidic control

The bioreactor is equipped with an individually controlled perfusion flow to all 10 sections to maintain the biochemical conditions including the transport of metabolites to and from the cell/scaffold construct. In addition to the circulation around the scaffold, culture medium will be led directly into the inner cores of the structured scaffold. This is accomplished by a perforated needle that is placed in the top mount, penetrating into the inner structures of the braided scaffold. Since the scaffold is an open-cell structure the media flows out of the scaffold again and merge with the fluid that surrounds the scaffold. Each reactor vessel has its own independent loop to allow different biochemical settings from one vessel to another and to avoid cross contamination. This fluid flow will be driven by a Gilson Minipuls Evolution peristaltic pump (Gilson Inc., Middleton, Wisconsin, USA).

To facilitate reproducible tissue growth, the environmental parameters (temperature, humidity) and influences from culture medium (pH, oxygen concentration, growth factors, and nutrients) need to be precisely controlled. Therefore the culture medium is placed in reservoir flasks in an incubator. These flasks are equipped with sterile membranes to guarantee gas exchange between culture medium and the gas mixture in the incubator. Flexible hoses lead from these flasks through the incubator to the bioreactor vessels. Steady pH (7.4), pO_2 (20%) or hypoxia can thus be maintained during cultivation.

To ensure a constant temperature (37°C) the vessels are surrounded with 15-watt heater mats (RS Components, Gmünd, Austria) controlled precisely via thermocouples TRFC101B (Correge, Pacy-sur-Eure, France) in conjunction with a Jumo Etron M temperature control unit (Jumo GmbH & Co. KG, Fulda, Germany).

2.4. Scaffold design

Another focus has been placed on the development of a novel silk fibroin protein matrix that matches ACL performance requirements. For that purpose we used white raw *Bombyx mori* silkworm fibres of 20/22 den, 250 T/m to braid a silk scaffold to withstand the mechanical properties of a native ACL.

To meet the mechanical demands and to consider all other necessary boundary conditions, we chose a braided structure which can be subdivided into a sheath and a core component, which composes of four

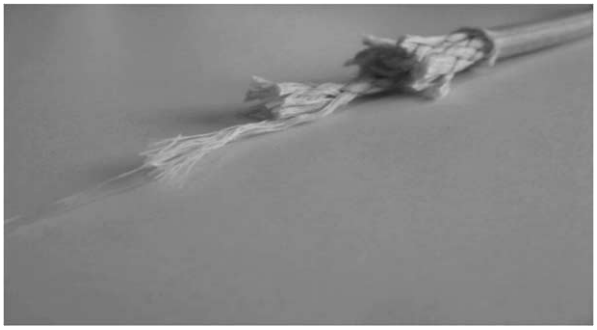

Fig. 4. Hierarchical structure of the silk scaffold.

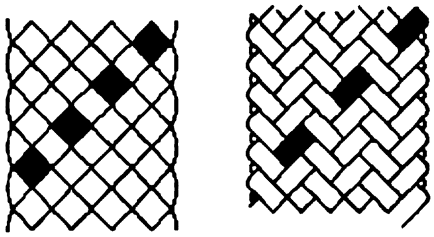

Fig. 5. Type of braid of the core bundles (*left*) and the sheathing (*right*).

strands. Both sheathing and core elements have a hierarchical structure composing of strands, bundles, twisted yarns and single silk fibres (see Fig. 4). Not only the sheath but also the core strands create a tubular braid. Six single silk fibres form a twisted yarn, which represents the basic raw material for braiding both the shell and the core strands. A bundle, which is processed in the sheathing, is composed of six twisted yarns, whereas core bundles contain twenty-four twisted yarns. These bundles in turn are the source material for braiding the tubular structures of the matrix. The sheathing and the strands result from this braiding procedure. The entire scaffold consists of the core component (four pieces of the strands) that is enclosed by the described tubular shell element.

The tubular design of the sheath and the core strands are made with a commercial braiding machine with fibres in every sixteen bobbins. Compared to the sheath, which has a braiding design according to the picture on the right (Fig. 5), the core strands are manufactured as the braid shown on the left. The braiding density of the sheathings and the core bundles reach 10 and 25 crossings/French inch, respectively. One French inch corresponds to 27.072 mm.

2.5. Degumming of silk scaffolds

The previously described pre-structured scaffolds were processed by extraction of sericin using an aqueous solution of 0.02 M Na_2CO_3 and 0.2% (w/v) SDS at 80–100°C for 1.5 h. Subsequently, they were rinsed thoroughly with distilled H_2O.

2.6. Mechanical testing of silk scaffolds

2.6.1. Mechanical properties

In order to evaluate the effects of the degumming process on our silk scaffolds in terms of alterations in the mechanical properties not only degummed scaffolds but also not degummed scaffolds were prepared for testing in wet and dry state:

- Type A: Not degummed silk scaffold, dry.
- Type B: Not degummed silk scaffold, wet.
- Type C: Degummed silk scaffold, dry.
- Type D: Degummed silk scaffold, wet.

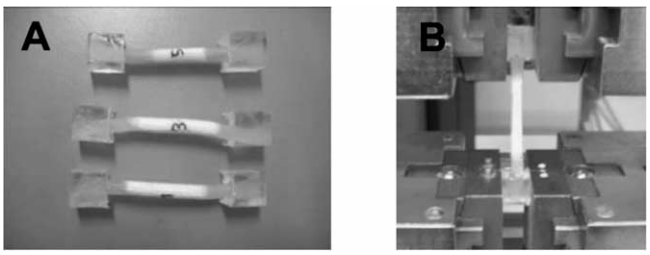

Fig. 6. (A) prepared scaffolds for mechanical testing; embedding of the ends in epoxy resin; (B) scaffold clamped in the mechanical testing machine.

From these different types, stress-strain curves were recorded using the material testing machine Zwick Z050 (Zwick GmbH & Co. KG, Ulm, Germany). Therefore the ends of the scaffolds were embedded in epoxy resin (epoxy resin L, R&G Faserverbundstoffe GmbH, Waldenbuch, Germany) to guarantee good locking in the testing machine (Fig. 6). Samples were pulled to failure at a strain rate of 5 mm/min to determine maximum loads, tensile strength and strains at failure. Due to the fact that the stiffness corresponds to the slope in the stress-elongation-curve the parameter can also be investigated.

All samples were tested at 23 $\pm$ 2°C and a relative humidity of 45–65%. Samples indicated as "wet" were incubated in a buffered solution (PBS) for at least 1 h prior to testing. After removal from the waterbath samples were immediately subjected to testing. Pull-to-failure tests were performed with 100 N of pretension.

2.6.2. Endurance testing

Endurance tests were performed using the bioreactor to analyze the long-term stability of the scaffolds. Before starting the cyclic motions for the duration of the experiment, the scaffold was pre-tensioned with 10 N. The axial displacement during the experiments was 3.5 mm (corresponding to an elongation of 7%), whereas the rotational movement was set to 45°. These parameters led to an approximate load of 300 N at a mechanical stimulation rate of 66.7 mHz.

2.6.3. Interaction of fibroblasts with scaffold material

If not indicated otherwise, all reagents were purchased from Sigma (Vienna, Austria) and of analytical grade. Preliminary studies of the interaction between fibroblasts and silk were performed using anterior cruciate ligament fibroblasts (ACLFs). These primary cells were isolated using a previously described [34] explant culture method from anterior cruciate ligaments collected from patients who were scheduled to undergo ACL replacement after rupture (IRB consent obtained).

A degummed silk cord was disassembled into single filaments. ACLFs were cultured in DMEM containing 10% fetal calf serum (FCS) (Lonza Ltd., Basel, Switzerland), 5% glutamine, 2% PenStrep and 100 µm L-ascorbic acid 2-phosphate in plates. ACLFs were seeded in 6 well-plates until 90% of confluence was reached. Then single filaments of a disassembled degummed silk cord with a length of 1 cm ($\sim$0.2 g) were added to each well of the 6-well plates. These plates were cultured for 48 h. Medium was aspirated and the respective medium containing 650 mg/ml MTT [3-(4,5-dimethylthiazol-2-yl)-2,5-diphenyltetrazolium] bromide was added to each well. Cells were incubated for 1 h in the incubator (37°C/5% CO_2). Then medium was aspirated and the MTT formazan precipitate was dissolved in 1 ml of DMSO by mechanical shaking in the dark for 20 min. Aliquots of 100 µl of each sample were pipetted into 96-well plates. The absorbances at 550 nm were read immediately thereafter on an automatic

microplate reader (Spectra Thermo, TECAN Austria GmbH, Austria). Optical density (OD) values were corrected for unspecific background.

In a different set of 6-well plates single filaments of a disassembled degummed silk cord with a length of 1 cm ($\sim$0.2 g) were seeded with a suspension of $0.5 \cdot 10^4$ ACLFs for 1 h. Then 2 ml of the above-quoted medium were added. After 24 h the filaments were observed via an Olympus CKX31 inverse microscope (Olympus GesmbH, Vienna, Austria).

2.7. Statistical analysis

Calculations were made using GraphPad software (GraphPad software, Inc., La Jolla, CA, USA). An unpaired t-test was used to calculate P-values for significance. $P < 0.05$ was considered statistically significant.

3. Results

3.1. Mechanical properties of silk scaffolds

The stress-strain curves of the treated and prepared scaffolds were record and are shown in Fig. 7. The results for these scaffolds are summarized in Table 1.

Not degummed samples have a higher maximum load than degummed scaffolds and wet scaffolds have a lower stiffness than dry samples. Due to the degumming process, the scaffolds had lost up to $\sim$28% of their mass ($n = 12$). The decreased maximum load of the degummed scaffolds can therefore be explained.

Since the lengthening of a human ACL amount to 0.1–3 mm [35,36] the stiffness was calculated in this elongation range. As a result of this study, not degummed, dry samples have the highest stiffness followed by degummed, dry and wet scaffolds.

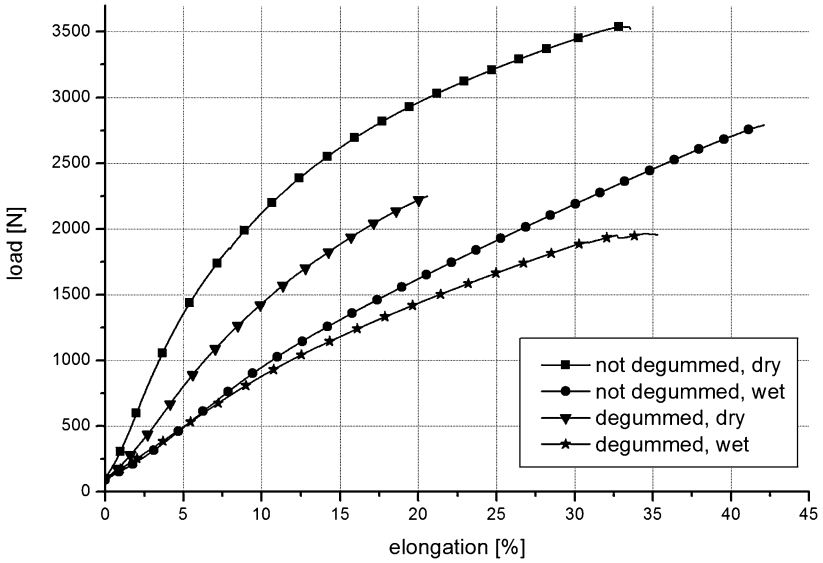

Fig. 7. Elongation vs. load of different type of silk scaffolds.

Table 1
Mechanical properties of the evaluated types of silk scaffolds

	Maximum load [N]	Tensile strength [N/mm^2]	Strain at failure [%]	Stiffness [N/mm]
Type A ($n = 3$)	3784 ± 197	143 ± 8	39 ± 2	717 ± 32
Type B ($n = 3$)	2840 ± 39	107 ± 2	43 ± 7	298 ± 44
Type C ($n = 4$)	2399 ± 176	91 ± 7	23 ± 5	500 ± 118
Type D ($n = 3$)	2023 ± 109	77 ± 4	35 ± 8	336 ± 40
Reference:	2160 ± 157			242 ± 28
Human ACL	[36]			[36]

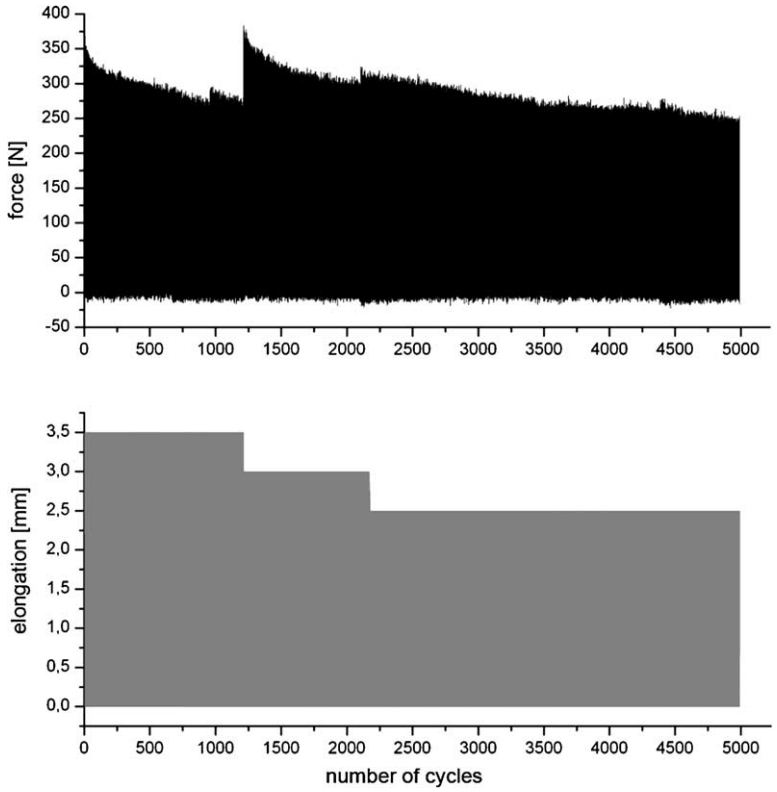

Fig. 8. Endurance test to analyze the scaffold stability, diagrams showing force [N] and elongation [mm] exerted on silk scaffold, respectively, vs. number of cycles applied.

3.2. Endurance test

Figure 8 shows the measured loads and the elongation of the scaffold vs. the number of cycles. Even though the functionality of the top and bottom anchoring systems was good, a slight slipping of the scaffold in the mounts had to be observed, which explains the decrease of the force in the diagram. Due to the fact, that the length of the scaffolds remained the same before and after testing, stress relaxation can be ruled out. In order to maintain a force level of approximately 300 N the scaffold was re-tensioned several times, which is visualized in Fig. 8. An improved version of the anchoring system which should avoid slipping and loosening of the scaffold system is currently under investigation.

3.3. Interaction of fibroblasts with scaffold material

Figures 9 and 10 show adherence to and coverage of the fibers with fibroblasts after 24 h of incubation, indicating the scaffold material to be a suitable substratum for ACLFs. Cells incubated with ∼0.2 g scaffold material showed no significant difference in cell viability compared to the control group (Fig. 11).

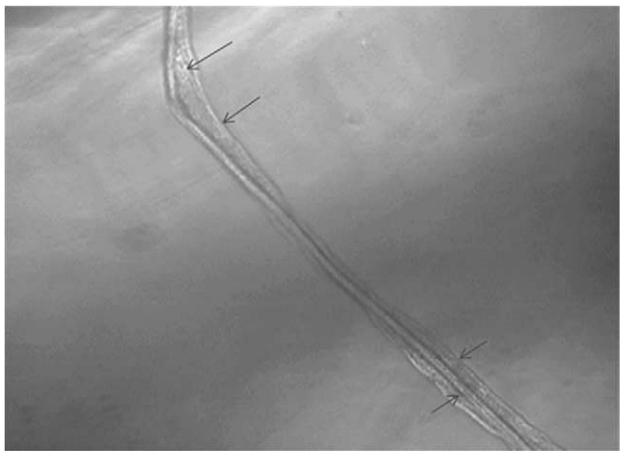

Fig. 9. A single silk fiber covered with ACL fibroblasts, arrows indicating fibroblasts.

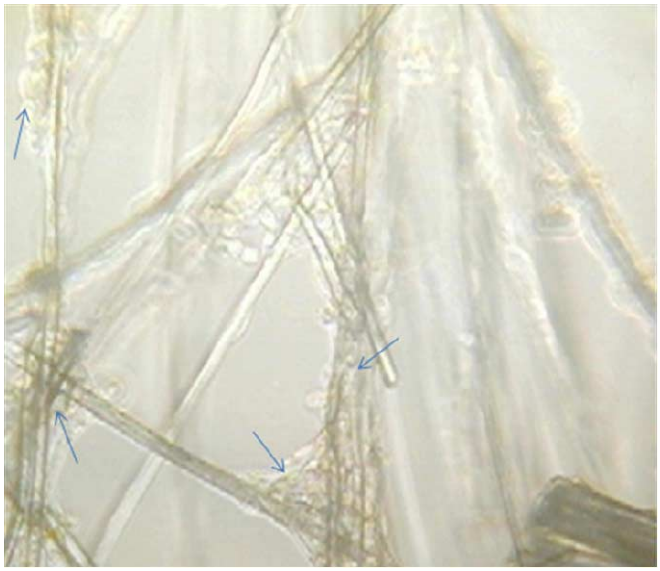

Fig. 10. Silk filaments covered with ACL fibroblasts, arrows indicating fibroblasts. (Colors are visible in the online version of the article; http://dx.doi.org/10.3233/BME-130746.)

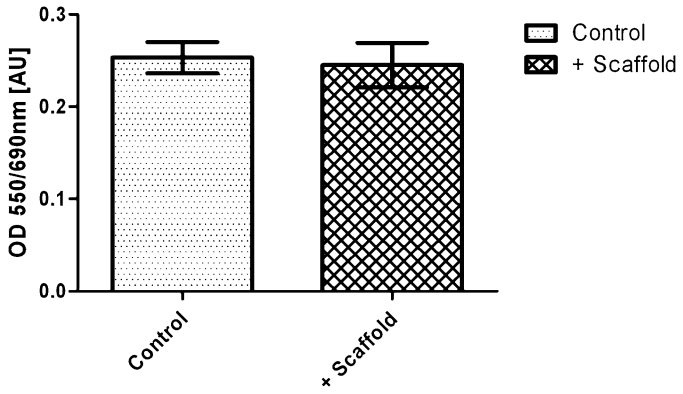

Fig. 11. Cell viability results of ACL fibroblasts cultured with scaffold material ($n = 6$). Controls were cells not cultured with scaffold material. Figure shows the mean values of OD $\pm$ STD.

4. Discussion

With this novel bioreactor system, cell and tissue growth on silk fibre matrices under both rotational and translational mechanical loading can be investigated.

Well-controlled mechanical strains (resolution of 3 μm for translational and 0.0075° for rotational movements) can be applied to the developing tissue while maintaining the complex biochemical and fluidic environments over prolonged periods of operation. The mechanical loading conditions thereby reflect the movement of the ACL in the human knee. The presented bioreactor surpasses the current state-of-the-art by its ability to apply mechanical stimulation separately to every five sections. An outstanding characteristic of the described bioreactor is the maximum axial tension of 1 kN that can be reached on each scaffold. Furthermore, the new individual tensioning system allows precise adjustments for every section prior to the experiments. With the force monitoring system, every alteration within the scaffold can be identified and recorded. A further innovative achievement is that culture medium is guided into the inner structures of the matrix to ensure uniform cell medium supply all over the scaffold.

While developing the bioreactor, we concentrated on the fabrication of an appropriate ACL silk scaffold.

To meet all the mechanical demands, our new scaffold has a special braided structure composing of strands, bundles, twisted yarns and single silk fibres. The raw scaffold reaches a maximum load of 3784 ± 197 N. After degumming, the utilized silk scaffolds have strength and stiffness values comparable to natural ligaments. Whereas a native ACL reaches a maximum load of 2160 ± 157 N [37], our wet and degummed structures show maximum loads of 2023 ± 109 N (Table 1). Furthermore, corresponding stiffness values could be found for our new silk scaffold (336 ± 40 N/mm vs. 242 ± 28 N/mm [37]). In the preliminary cell culture experiments we were able to demonstrate that our silk scaffold material is a suitable substratum for ACL fibroblasts regarding adhesion capability and cell viability. In future studies ACL fibroblasts will be used as a fibroblastic cell line to compare the effects of mechanical loads on the differentiation and proliferation of bone marrow derived stem cells (BMSC). The main advantage of BMSCs over ACL fibroblasts is their higher growth rate. Therefore they can be considered an alternative cell source for ACL tissue engineering [19].

5. Conclusion

This new, elaborate bioreactor was designed to perform endurance tests with various (cell-seeded) ACL grafts, in which the physiological mechanical conditions of an anterior cruciate ligament are closely mirrored. An integrated, well-controlled biochemical and fluidic control system of the bioreactor guarantees an optimal environment for the developing tissue. Beside endurance testing, this system also permits analysis of the interactions between different cell types and scaffolds under accurate and precisely controlled multi-dimensional mechanical stimulation. Furthermore, a scaffold manufactured of *Bombyx mori* silk was designed exhibiting a three-dimensional braided structure matching the mechanical properties of a native human ACL. Further studies will focus on the cultivation of different cell types on our custom-made silk scaffold under distinct mechanical stimulation regimes and evaluate their potency as a cell source for a tissue engineered approach of ACLs.

Acknowledgement

Financial support by the Austrian Research Agency FFG under the contract 815471 is greatly acknowledged.

References

[1] K.R. Reinhardt, I. Hetsroni and R.G. Marx, Graft selection for anterior cruciate ligament reconstruction: A level I systematic review comparing failure rates and functional outcomes, *Orthop. Clin. B Am.* **41** (2010), 249–262.
[2] S.U. Scheffler, N.P. Südkamp, A. Göckenjan, R.F.G. Hoffmann and A. Weiler, Biomechanical comparison of hamstring and patellar tendon graft anterior cruciate ligament reconstruction techniques: the impact of fixation level and fixation method under cyclic load, *Arthroscopy* **18**(3) (2002), 304–315.
[3] R.J. Williams III, J. Hyman, F. Petrigliano, T. Rozental and T.L. Wickiewicz, Anterior cruciate ligament reconstruction with a four-strand hamstring tendon autograft, *JBJS* **86-A** (2004), 225–232.
[4] C.C. Prodromos, Y.S. Han, B.L. Keller and R.J. Bolyard, Stability results of hamstring anterior cruciate ligament reconstruction at 2- to 8-year follow up, *Arthroscopy* **21**(2) (2005), 138–146.
[5] S.M. Howell, Rationale and endoscopic technique for anatomic placement and rigid fixation of a double-looped demitendinosus and gracilis graft, *Techniques in Orthopedics* **13**(4) (1998), 319–328.
[6] R.V. Larson, Complications and pitfalls in anterior cruciate ligament reconstruction with hamstring tendons, in: *Knee Surgery: Complications, Pitfalls, and Salvage*, M. Malek, ed., Springer-Verlag, New York, 2000.
[7] D.A. McGuire and S.D. Hendricks, Allograft tissue in ACL reconstruction, *Sports Med. Arthrosc. Rev.* **17**(4) (2009), 224–233.
[8] F.A. Barbera, J. Aziz-Jacobo and F.B. Oro, Anterior Cruciate ligament reconstruction using patellar tendon allograft: an age-dependent outcome evaluation, *Arthroscopy* **26**(4) (2010), 488–493.
[9] R.W. Nutton, I. McLean and E. Melville, Tendon allografts in knee ligament surgery, *J. R. Coll. Surg. Edinb.* **44**(4) (1999), 236–240.
[10] R.K. Peterson, W.R. Shelton and A.L. Bomboy, Allograft versus autograft patellar tendon anterior cruciate ligament reconstruction: A 5-year follow-up, *Arthroscopy* **17**(1) (2001), 9–13.
[11] M.H. Gretelman and M.J. Friedmann, Complications and pitfalls in anterior cruciate ligament reconstruction with synthetic grafts, in: *Knee Surgery: Complications, Pitfalls, and Salvage*, M. Malek, ed., Springer-Verlag, New York, 2000.
[12] G. Hehl, L. Kinzl and R. Reichel, Carbon-fiber implants for knee ligament reconstruction. 10-year results, *Chirurg* **68**(11) (1997), 1119–1125.
[13] L.E. Paulo et al., The GORE-TEX anterior cruciate ligament prosthesis. A long-term followup, *Am. J. Sports Med.* **20**(3) (1992), 246–252.
[14] M. Hohlrieder and J. Stampfl, Endurance strength of artificial ligament materials, *Tissue Engineering Part A* **14**(5) (2008), 847–848.
[15] G.H. Altman et al., Silk matrix for tissue engineered anterior cruciate ligaments, *Biomaterials* **23**(20) (2002), 4131–4141.
[16] R.L. Horan et al., Yarn design for functional tissue engineering, *J. Biomech.* **39**(12) (2006), 2232–2240.

[17] R.E. Unger et al., Growth of human cells on a non-woven silk fibroin net: a potential for use in tissue engineering, *Biomaterials* **25**(6) (2004), 1069–1075.
[18] G.H. Altman et al., Silk-based biomaterials, *Biomaterials* **24**(3) (2003), 401–416.
[19] Y. Wang et al., Stem cell-based tissue engineering with silk biomaterials, *Biomaterials* **27**(36) (2006), 6064–6082.
[20] G.H. Altman et al., Advanced bioreactor with controlled application of multi-dimensional strain for tissue engineering, *J. Biomech. Eng.* **124**(6) (2002), 742–749.
[21] C.J. Kahn et al., A novel bioreactor for ligament tissue engineering, *Biomed. Mater. Eng.* **18**(4–5) (2008), 283–287.
[22] F. Grinnell, Fibroblasts, myofibroblasts, and wound contraction, *J. Cell Biol.* **124**(4) (1994), 401–404.
[23] D. Mooney et al., Switching from differentiation to growth in hepatocytes: control by extracellular matrix, *J. Cell. Physiol.* **151**(3) (1992), 497–505.
[24] J.L. Schwachtgen et al., Fluid shear stress activation of egr-1 transcription in cultured human endothelial and epithelial cells is mediated via the extracellular signal-related kinase $1/2$ mitogen-activated protein kinase pathway, *J. Clin. Invest.* **101**(11) (1998), 2540–2549.
[25] S. Diederichs et al., Dynamic cultivation of human mesenchymal stem cells in a rotating bed bioreactor system based on the Z RP platform, *Biotechnol. Prog.* **25**(6) (2009), 1762–1771.
[26] M. van Griensven et al., Mechanical strain using 2D and 3D bioreactors induces osteogenesis: Implications for bone tissue engineering, *Adv. Biochem. Eng. Biotechnol.* **112** (2009), 95–123.
[27] S.W. Cho et al., Smooth muscle-like tissues engineered with bone marrow stromal cells, *Biomaterials* **25**(15) (2004), 2979–2986.
[28] J. Garvin et al., Novel system for engineering bioartificial tendons and application of mechanical load, *Tissue Eng.* **9**(5) (2003), 967–979.
[29] E. Langelier et al., Cyclic traction machine for long-term culture of fibroblast-populated collagen gels, *Ann. Biomed. Eng.* **27**(1) (1999), 67–72.
[30] K.A. Peperzak, T.W. Gilbert and J.H. Wang, A multi-station dynamic-culture force monitor system to study cell mechanobiology, *Med. Eng. Phys.* **26**(4) (2004), 355–358.
[31] L.H. Yahia, E.A. Desrosiers and C.H. Rivard, A computer-controlled apparatus for *in vitro* mechanical stimulation and characterization of ligaments, *Biomed. Mater. Eng.* **1**(4) (1991), 215–222.
[32] J. Chen et al., Human bone marrow stromal cell and ligament fibroblast responses on RGD-modified silk fibers, *J. Biomed. Mater. Res. A* **67**(2) (2003), 559–570.
[33] M. Hohlrieder et al., Bioreactor and scaffold design for the mechanical stimulation of silk based anterior cruciate ligament grafts, in: *World Congress on Medical Physics and Biomedical Engineering; IFMBE Proceedings*, W.S.O. Dössel, ed., München, 2009.
[34] C.N. Nagineni, D. Amiel, M.H. Green, M. Berchuck and W.H. Akeson, Characterization of the intrinsic properties of the anterior cruciate and medial collateral ligament cells: an *in vitro* cell culture study, *J. Orthop. Res.* **10**(4) (1992), 465–475.
[35] B.D. Beynnon, B.S. Uh, R.J. Johnson, B.C. Fleming, P.A. Renström and C.E. Nichols, The elongation behavior of the anterior cruciate ligament graft *in vivo*, *Am. J. Sports Med.* **29**(2) (2001), 161–166.
[36] G. Li, L.E. DeFrate, H. Sun and T.J. Gill, *In vivo* elongation of the anterior cruciate ligament and posterior cruciate ligament during knee flexion, *Am. J. Sports Med.* **32** (2004), 1415–1420.
[37] F.R. Noyes et al., Biomechanical analysis of human ligament grafts used in knee-ligament repairs and reconstructions, *J. Bone Joint Surg. Am.* **66**(3) (1984), 344–352.